Available online at www.sciencedirect.com
ScienceDirect
Engineering Fracture Mechanics 75 (2008) 1507–1515
Engineering Fracture Mechanics
www.elsevier.com/locate/engfracmech

Mechanics of two-stage crack growth in fretting fatigue

B. Yang [a,*], S. Mall [b]

[a] Department of Mechanical and Aerospace Engineering, Florida Institute of Technology, Melbourne, FL 32901, United States
[b] Department of Aeronautics and Astronautics, Air Force Institute of Technology, Wright-Patterson AFB, Dayton, OH 45433, United States

Received 28 March 2007; received in revised form 25 June 2007; accepted 26 June 2007
Available online 15 August 2007

Abstract

Motivated by experimental observations, we carry out a numerical analysis of the two-stage crack growth under fretting fatigue by using an efficient and accurate boundary element method. To start with, the variation of stress field during a loading cycle is analyzed. Various values of friction coefficient in the contact zone are considered, which is shown to considerably affect the stress field. Then, by assuming crack initiation to occur in the shear mode, a surface-breaking crack is introduced to the specimen at the location of highest shear-stress amplitude. The crack-tip stress intensity factors (SIFs) are calculated for various crack lengths and at various crack angles ranging from 25° to 45° about the contact surface. It is shown that, for a loading ratio of 0.5, the cyclic mode-II SIF amplitude decreases with increasing crack length, whilst its mean value increases. It suggests that the (first-stage) shear crack would sooner or later become dormant, or switch to another mode that can provide continuous support of growth. Then, the first-stage shear crack is manually kinked into a second-stage opening crack, and the follow-on driving force is analyzed. It is shown that the kinking event is only favored after the first-stage crack has grown to a certain length. The present study thus provides insights in the mechanics of two-stage crack growth that has been frequently observed in a typical dovetail joint under fretting fatigue. It also suggests an improved experimental setup to quantitatively investigate the fretting fatigue in dovetail joints.

Keywords: Boundary element method; Contact mechanics; Crack initiation; Crack kinking; Dovetail joints; Fracture mechanics; Friction; Fretting fatigue

1. Introduction

Severe stress state emerges in the contact zone between two mating components, causing localized plastic deformation and damage. If loading is cyclic, it becomes more hazardous, leading to crack initiation and growth [4,7,13,16,22,23]. This damage process including crack development is referred to as fretting fatigue. It has been practically divided into two phases, namely, initiation and propagation phases, depending upon the size of a crack that can be detected by available nondestructive evaluation techniques. The initiation phase involves early crack growth up to a few hundreds of microns. Meanwhile, the propagation phase is the follow-on growth of cracks until structural failure. In the initiation phase, the cracks are often found to develop at an

* Corresponding author.
E-mail address: boyang@fit.edu (B. Yang).

0013-7944/$ - see front matter © 2007 Elsevier Ltd. All rights reserved.
doi:10.1016/j.engfracmech.2007.06.009

inclination from the contact surface. Then, they kink and eventually propagate normal to the bulk tension, exhibiting a typical two-stage crack initiation and growth pattern [4,10,19,21].

To characterize the fretting-fatigue crack initiation, Fellows et al. [5] utilized the shear-stress amplitude as the key parameter in a stress-based approach. Lykins et al. [11,12] later showed through a combined numerical and experimental analysis with cylinder-on-flat and flat-on-flat contact configurations that the sites of fretting-fatigue crack initiation can indeed be reasonably explained with this parameter. Furthermore, Yang and Mall [25] applied the crack analogue model/fracture-mechanics approach [6] to study the driving forces for initiation of mode-I and mode-II cracks at the edge of contact with friction coefficient in the contact zone as the key parameter. By comparing with experimental observations, they showed that the fretting-fatigue crack initiation was in the shear mode.

On the other hand, the observed kinking of an initiated fretting-fatigue crack suggests a transition of fracture mechanism from a shear to an opening mode. A few fracture-mechanics-based approaches have been utilized to analyze fretting-fatigue crack initiation and growth, without separating them, under either opening-mode or mixed-mode condition along a prescribed path [2,14,15]. However, a parametric study of the two-stage cracking process in fretting fatigue has not been reported in the literature. Meanwhile, a number of critical plane-based approaches without any consideration of fracture-mechanics principles have been proposed to predict the crack-initiation life based on the stress/strain amplitude at the contact surface before the crack initiation [5,9,18,22]. These critical-plane-based approaches could be improved if a two-stage crack initiation and early growth consideration is included. This has motivated the present study.

In the present work, we numerically simulate the two-stage cracking process in fretting fatigue guided by experimental observations. To start with, the variation of stress field during a typical loading cycle is analyzed. Various values of friction coefficient in the contact zone are examined, which is shown to considerably affect the stress field. Then, a surface-breaking shear-mode crack is introduced at the location of highest shear-stress amplitude in the contact zone. The crack-tip stress intensity factor (SIF) is calculated for various crack lengths and various crack orientation angles ranging from 25° to 45° about the contact surface. It is then manually kinked into an opening crack based on the criterion of maximum tangential-stress amplitude. This parametric study suggests that the crack should become dormant, or switch from the shear to an opening mode by kinking, after a certain distance of propagation. This is consistent with the experimental observations. In Section 2, the nonlinear problem of frictional contact and crack is formulated. It is solved by applying the boundary element (BE) method [1,24]. In Section 3, the stress field in the contact zone before crack initiation is analyzed for various fretting-fatigue parameters including the loading ratio and the friction coefficient. In Section 4, the two-stage process of fretting-fatigue crack initiation and early growth is analyzed. In Section 5, conclusions are drawn.

2. Problem formulation

One of the major concerns and considerations in the design of a dovetail joint, for example, used to connect a blade to a disk in gas turbine engines (Fig. 1a), is fretting fatigue. When a cyclic loading is applied, the force

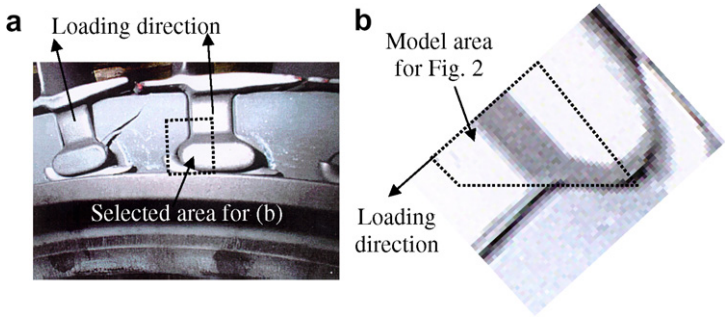

Fig. 1. (a) A typical dovetail joint connecting a blade and a disk in a turbine engine. (b) A selected window area of (a) upon rotation.

acting in the contact zone between the connected parts (blade and disk) varies in both normal and tangential components. The two components are coupled in a way determined by the geometry of the joint. However, it was often experimentally studied with a fretting test setup, as well as analytically, where the normal force component (or normal displacement component) is held constant while the tangential force component is varied ([3,4,9,16,17], among many others). The realistic geometry of a dovetail joint has also been taken into account in several fretting-fatigue studies [8,18,20]. In the present study, we consider a configuration where the normal and tangential loading components are coupled, as shown in Fig. 2. It represents more closely the realistic condition in a dovetail joint, as shown in Fig. 1b, a part of Fig. 1a. Furthermore, the setup may be realized in a laboratory as easily as the previous ones.

The setup shown in Fig. 2 consists of two parts: a specimen, and a component to apply fretting loads to the specimen through a pad. In our simulation, the specimen and loading component are taken to be the same material, and it is isotropic and linearly elastic. The specimen is restrained by a smooth sliding guide of a rigid wall along its bottom and right boundaries. The loading component is subjected to a normal traction σ along its left boundary, and is allowed to slide smoothly along the top boundary against a rigid wall. The loading component is initially in touch, through a cylindrical pad, with the flat top surface of specimen, but without pre-stress. Because of the wedge shape of the loading component, the pad and the specimen top surface come in contact over a finite zone when σ is applied. The structure is free of traction otherwise. The boundary conditions and other details are shown schematically in Fig. 2. The loading direction, β, may be adjusted for desired fitting tightness between the loading component and the specimen, which closely represent the parts of a blade and a disk in a dovetail joint, respectively.

When the setup (Fig. 2) is subjected to fatigue loading, i.e. cyclic σ, a crack may nucleate at the contact surface in the specimen. The crack may be opened, closed, or partially both during a loading cycle. The non-penetration condition of opposite surfaces is enforced upon a closed crack as well as between the pad and the specimen. The tangential interaction between contact surfaces is modeled by a Coulomb-type friction law,

$$\tau = fp\frac{\dot{w}}{|\dot{w}|}, \tag{1}$$

where τ and p are the tangential and normal components of traction, f is the friction coefficient, $\dot{w}$ is the time rate of change of relative displacement between the surfaces in contact, and $|\dot{w}|$ is its magnitude. The traction components, τ and p are defined with the specimen.

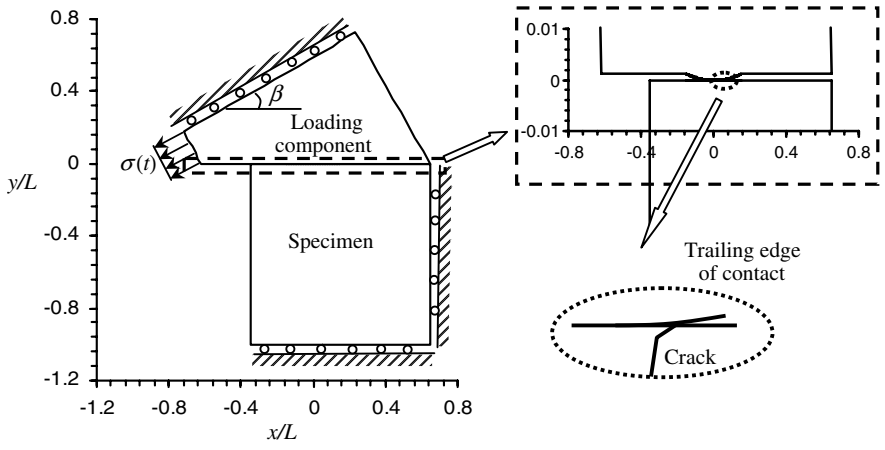

Fig. 2. A setup simulating a dovetail joint (Fig. 1) under fretting fatigue. The inserts show a cylindrical pad of loading component and a crack possibly initiating and growing at the trailing edge of contact. The dimensions are scaled by a characteristic length scale L.

Since the material is linearly elastic (and isotropic), the displacement at a boundary point can be expressed as an integral of weighted displacement and traction along the boundary and crack. It is given for the loading component and for the specimen, respectively, as

$$\frac{1}{2}u_i = \int_{\Gamma^{(\mathrm{ld})}} [u^*_{ij}p_j - p^*_{ij}u_j]\mathrm{d}\Gamma, \tag{2}$$

$$\frac{1}{2}u_i = \int_{\Gamma^{(\mathrm{sp})}} [u^*_{ij}p_j - p^*_{ij}u_j]\mathrm{d}\Gamma + \int_{\Gamma^{(\mathrm{cr})}} p^*_{ij}w_j\mathrm{d}\Gamma, \tag{3}$$

where $\Gamma^{(\mathrm{ld})}$ and $\Gamma^{(\mathrm{sp})}$ are the boundaries of the loading component and the specimen, respectively, $\Gamma^{(\mathrm{cr})}$ is one side of a crack, u is the displacement, p is the traction, w is the displacement jump across a crack, and u^*_{ij} and p^*_{ij} are the fundamental solutions of displacement and traction of isotropic elasticity [1]. To solve the crack problem in a single-domain formulation, the following integral equation of traction is required,

$$p_i = \int_{\Gamma^{(\mathrm{sp})}} [U^*_{ij}p_j - P^*_{ij}u_j]\mathrm{d}\Gamma + \int_{\Gamma^{(\mathrm{cr})}} P^*_{ij}w_j\mathrm{d}\Gamma \tag{4}$$

where U^*_{ij} and P^*_{ij} are combinations of derivatives of u^*_{ij} and p^*_{ij}, which can be found in [1] as well. The above Equations (2)–(4) can be used to develop an efficient and accurate BE method to numerically solve the above nonlinear boundary-value problem. One may refer to [1] for general details of the numerical technique, and [24] for particular treatment of the nonlinear problem of frictional contact and crack. An iterative scheme is necessary to solve the present nonlinear problem.

3. Contact stress analysis

In the following simulations, we set the loading direction $\beta = 30°$, radius of the cylindrical pad $r = 10L$, and other geometrical parameters as shown in Fig. 2, where L is a length scale used to normalize all quantities of the dimension of length. A change in β or in r would affect significantly the magnitude but affect very little the characteristics of the stress field in the contact zone. The Young's modulus E is used to normalize all quantities of the dimension of stress. The Poison's ratio v is set equal to 0.3. We adopted an adaptive mesh with concentration of elements in and around the contact zone. The following solutions had all been subjected to a convergence check with mesh refinement. The final mesh is such that when the mesh density is doubled, the relative change of displacement is less than 0.1%.

The first simulation was run with the system being loaded monotonically up to $\sigma = 0.005E$, and then unloaded completely. The friction coefficient in the contact zone $f = 0.3$. Stresses along the contact surface of the specimen are recorded at the peak load and three intermediate unloading levels. The results are plotted in Fig. 3a–d. In Fig. 3a, the system is subjected to the peak load. The variation of shear traction component τ_{xy} indicates that the contact zone is in the full slipping condition, i.e. under the gross slip condition. The tangential-stress component σ_x is tensile and concentrated at the trailing edge of contact, but is compressive (without concentration) at the leading edge of contact. Fig. 3b–d shows the stress state after unloading. During the unloading process, the pressure, i.e. the normal traction component σ_y decreases. Reversed slip occurs at both of the contact edges, with a stick zone inside. The stick zone recedes gradually and diminishes. The tangential stress component σ_x at the trailing edge of contact (tensile at the peak load) quickly turns into compression. However, the tangential-stress component at the leading edge of contact (compressive at the peak load) turns into tension, showing a slight concentration, and finally diminishes. These figures show the characteristics of contact stress variation during a loading cycle before crack initiation in the setup simulating a dovetail joint as well as the accuracy of the numerical solution.

To understand the role of friction, another simulation was run with the same parameters as above except for the friction coefficient in the contact zone being changed to 0.7. The system was loaded up monotonically to the peak load and then unloaded to the half way down, i.e., loading ratio $R = 0.5$. Stresses along the contact surface at the peak load and the final unloading point are plotted in Fig. 4a and b. Compared to the previous case, a smaller contact zone with lower contact pressure σ_y, higher shear traction component τ_{xy}, and higher tangential (tensile) stress σ_x concentration at the trailing edge of contact are observed with higher value of

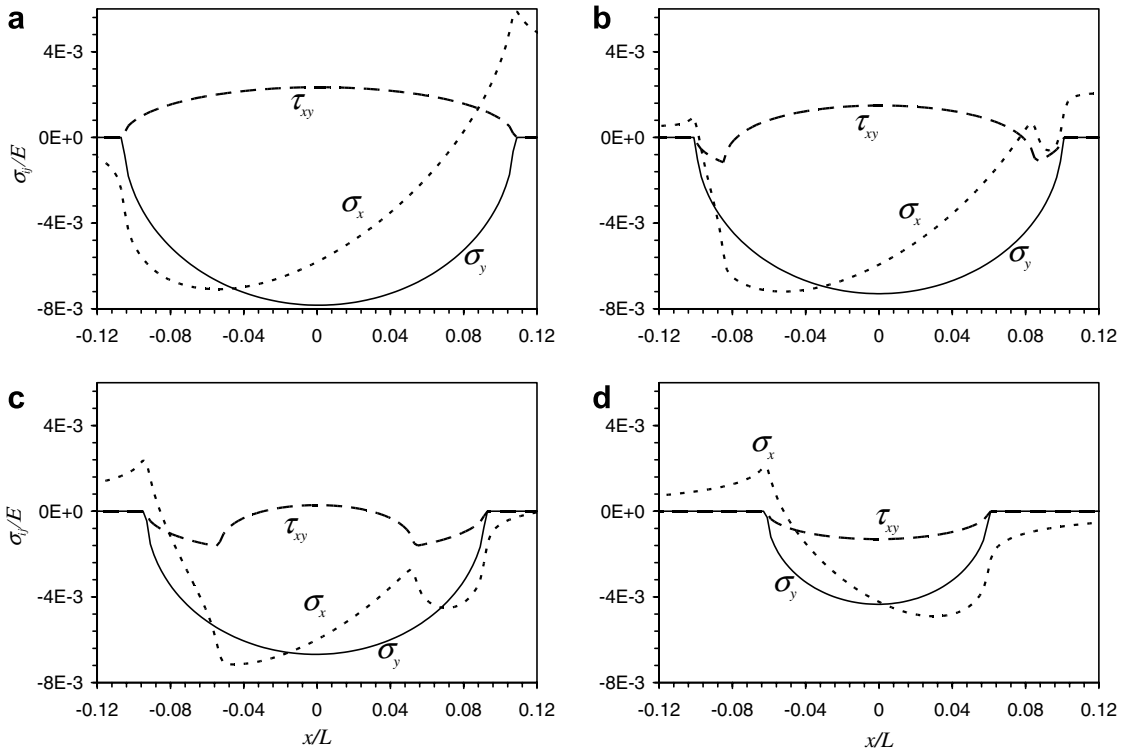

Fig. 3. Variation of stress components (normalized by Young's modulus E) along contact surface at (a) (peak load) $\sigma = 0.005\ E$; (b) (unloaded) $\sigma = 0.0035\ E$; (c) $\sigma = 0.002\ E$; and (d) $\sigma = 0.0005\ E$. In the case, $f = 0.3$.

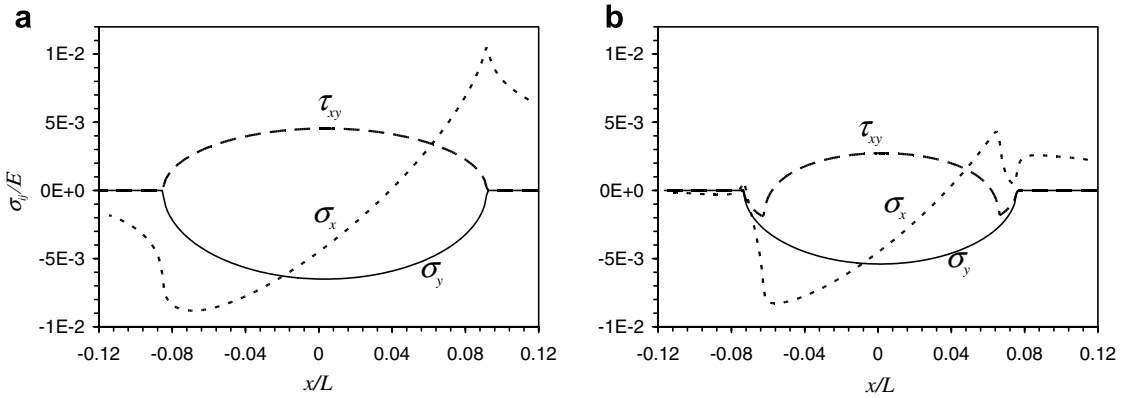

Fig. 4. Variation of stress components (normalized by Young's modulus E) along contact surface at (a) (peak load) $\sigma = 0.005\ E$ and (b) (unloaded) $\sigma = 0.0025\ E$. In the case, $f = 0.7$.

friction coefficient f in the contact zone. However, there appears to be little change in the qualitative features of the stress distribution along the contact surface.

To prepare for the next analysis of two-stage crack growth, the amplitude of stress oscillation is examined with loading ratio $R = 0.5$ and friction coefficient $f = 0.3$ and 0.7. Variations of the maximum normal-stress amplitude, the maximum shear-stress amplitude, and angle of the maximum shear-stress amplitude along the contact surface are plotted in Figs. 5 and 6a and b, respectively. The angle of the maximum normal-stress amplitude is equal to the angle of the maximum shear-stress amplitude plus 45°. First, it is seen that the trailing edge of contact experiences more severe fatigue loading than the leading edge of contact. Thus, the next

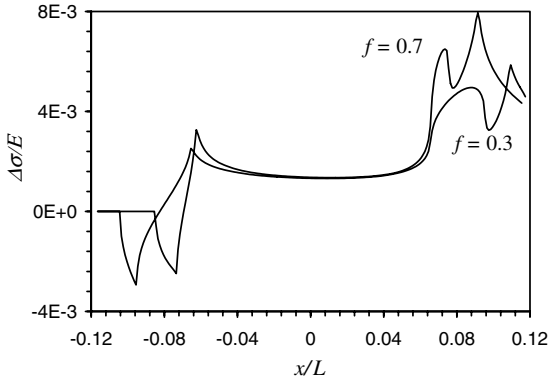

Fig. 5. Variation of maximum normal-stress amplitude along contact surface with friction coefficient $f = 0.3$ and 0.7.

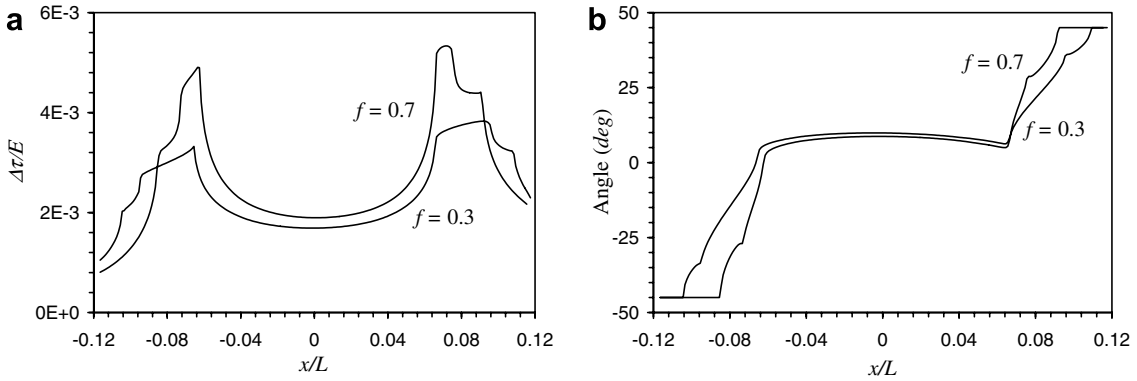

Fig. 6. Variation of (a) maximum shear-stress amplitude and (b) corresponding angle along contact surface with friction coefficient $f = 0.3$ and 0.7.

step of crack analysis will focus on the former. It is also seen that there are two peaks of the maximum normal-stress amplitude. There exists a higher peak at the edge of contact at the peak load, and a lower one within the reversed slip zone after unloading (at one half of the peak load). There is only one peak of the maximum shear-stress amplitude in the reversed slip zone. Most importantly, it is shown that both of the maximum normal and the maximum shear-stress amplitudes exhibit higher magnitude and higher gradient with greater value of friction coefficient in the contact zone. Thus, the resulting stress field would be increasingly hazardous for crack initiation during fretting fatigue as the magnitude of friction coefficient increases (due to surface roughening). In addition, the angle of the maximum shear-stress amplitude varies from about 5° to 45° with location from the reversed stick-slip boundary to the trailing edge of contact at the peak load.

4. Crack analysis

In the section, we examine the process of two-stage fretting-fatigue crack growth in a dovetail-joint-like configuration as shown in Fig. 2. The case of friction coefficient in the contact zone equal to 0.7 and loading ratio equal to 0.5 that was studied before cracking in the previous section is considered here. To conduct the crack analysis, a surface-breaking crack is introduced to the specimen at the location of highest shear-stress amplitude and at various angles ranging from 25° to 45° about the contact surface. This range of angles is chosen because in those planes, appreciable shear-stress amplitude has been observed, as shown in Fig. 6. Appreciable shear-stress amplitude has been found for angles between 5° and 25° as well. However, in this range of angles, the initial crack is always closed for the range of crack length examined. Thus, it is not considered in the following discussion. The location of the initial crack is fixed at the location of highest

shear-stress amplitude because through extensive simulations with initial crack location about it, the crack behavior was found to be insensitive to the location. The crack surfaces are assumed to be frictionless for the sake of simplicity of discussion. The crack-surface friction is believed to alter only quantitatively the following discussion. The crack-tip SIFs are calculated for various crack lengths at the instances of maximum and minimum loads. At the instant of minimum load, the cracks are all closed. At the instant of peak load, the crack is closed for all the lengths considered if the angle is equal to 25°. For angles greater than that, the cracks are open at small lengths, but are closed at longer lengths. The variations of the mean value and the amplitude of the cyclic mode-II SIF along the crack paths are plotted in Fig. 7. Meanwhile, the variation of the mode-I SIF at the peak load with crack length is plotted in Fig. 8.

It is shown in Fig. 7 that the mean mode-II SIF increases with crack length. It is insensitive to the crack angle in the range from 25° to 45°. On the other hand, the mode-II SIF amplitude varies significantly with crack angle up to 40°. When the crack angle is greater than 40° (and smaller than 45° under consideration) the difference becomes insignificant. In all these cases, the mode-II SIF amplitude initially increases and then decreases with crack length. It means that the crack would be arrested after reaching a certain length if the process is governed only by this parameter. Or, it would switch to the opening mode, or any mixed mode, that can provide continuous support of growth. The sharp kinks in curves in Figs. 7 and 8 correspond to the instance when the crack initially open at the peak load has grown long enough and turns into a completely closed crack during a loading cycle. This is evident in Fig. 8 where the opening mode-I SIF normal to the crack becomes zero. The history of the mode-I SIF is shown here because its magnitude is comparable to that of mode-II SIF amplitude. It may provide assistance to the mode transition during the growth of an initial shear crack.

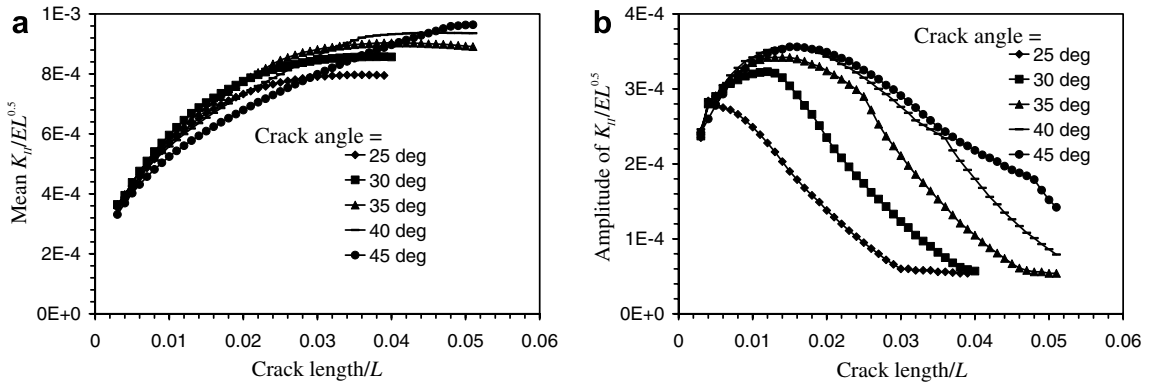

Fig. 7. Variation of (a) mean value and (b) amplitude of mode-II SIF with crack length at various crack angles.

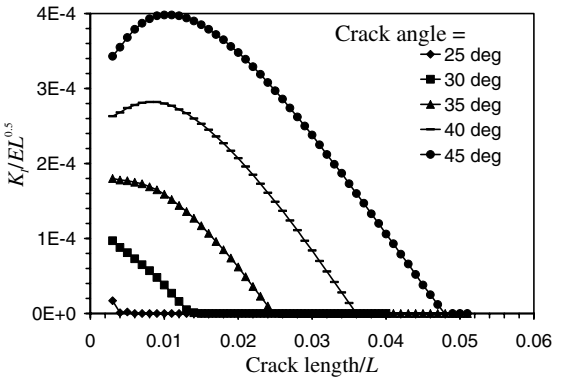

Fig. 8. Variation of mode-I SIF with crack length at peak load at various crack angles.

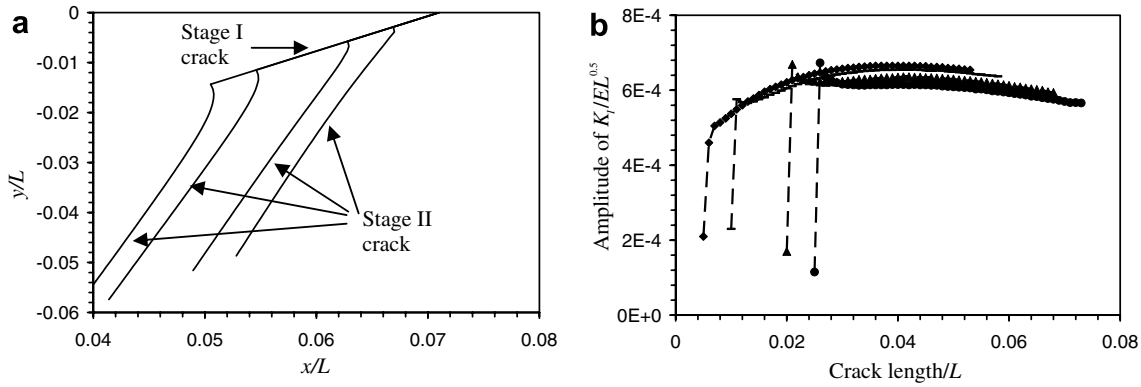

Fig. 9. (a) Crack paths of a two-stage crack kinked at various first-stage crack lengths. (b) Mode-I SIF amplitude along the paths.

Another set of simulations are conducted where the initial shear crack is forced to turn into an opening crack at various depths according to the maximum tangential-stress criterion. Then, the crack is allowed to grow in the opening mode by the same criterion. Note that the criterion in terms of the SIF amplitude is applied, i.e. the crack propagates along the direction of the maximum mode-I SIF amplitude and zero mode-II SIF amplitude. However, the mode-II SIF itself may be nonzero. For example, Fig. 9a shows the two-stage crack trajectories with various kinking depths. The first-stage crack is inclined at 35°. Meanwhile, Fig. 9b shows the mode-I SIF amplitude along the crack trajectories. It is seen that the cracks, in all cases, kink in the direction of 73° from the contact surface. This is the direction of maximum bulk tensile stress amplitude. Furthermore, the mode-I SIF amplitude is insensitive to the kinking depth, and there appears to be a master curve for all these cases of different kinking depths. Along this master curve, the mode-I SIF amplitude first increases and then decreases with crack length. This shows the transition of early crack growth from a region where contact stress dominates to a region where its effect diminishes. Finally, it clearly indicates that the kinking process is favored only after the first-stage shear crack has grown to a certain depth. The mechanics of fretting-fatigue crack growth in two stages discussed above should hold qualitatively invariant with loading direction, β or pad radius, and thus a detailed parametric study in terms of those parameters is unnecessary. Certainly, they are important in the practical design.

In summary, the first-stage shear crack, after its initiation, experiences a decreasing driving force with growth. Before the driving force of mode-II crack growth becomes ineffective, the crack would switch to an opening mode if the driving force for the transition suffices. Otherwise, it would become dormant, i.e. it would be arrested. The revealed mechanics of two-stage process of early fretting-fatigue crack growth in the present study is consistent with the previous extensive experimental observations as cited before. It may be extended to model/predict the early fretting-fatigue crack growth in dovetail joints in turbine engines by taking into account realistic geometry and loading conditions.

5. Conclusions

We have carried out a numerical BE analysis of the two-stage cracking process in fretting fatigue. First, the contact stress field in a dovetail-joint-like setup was analyzed for various fretting-fatigue parameters including fatigue loading ratio and friction coefficient in the contact zone. For instance, in the case of loading ratio equal to 0.5, the maximum shear-stress amplitude is shown to occur near the slip-stick boundary at the instant of minimum load and at the trailing edge of contact at the instant of peak load. The corresponding angle, i.e. corresponding plane at which the maximum shear-stress amplitude acts, ranges from 5° to 45° from the contact surface. Both of the maximum normal and the maximum shear-stress amplitudes are concentrated at the leading and trailing edges of contact – more severe at the latter location.

Then, a crack was introduced to the specimen at the location of highest shear-stress amplitude. The crack-tip SIFs were calculated for various crack orientation angles and lengths. It was shown that the mode-II SIF

amplitude first increases and then decreases with increasing crack length, whilst its mean value increases. This suggests that the first-stage crack would be arrested, or keep on growing by switching to the opening mode. Thus, an initial shear crack was manually kinked at various depths. Along the crack path after kinking, the mode-I SIF amplitude is shown to increase initially but decrease later on. It suggests that the first-stage small-angle shear crack would sooner or later become dormant/be arrested, or switch to the opening mode in which its fatigue growth can continue. All these numerical results agree well (qualitatively) with the previous experimental observations.

References

[1] Brebbia CA, Telles JCF, Wrobel LC. Boundary element techniques: theory and applications in engineering. Springer-Verlag; 1984.
[2] Chan KS, Lee YD, Davidson DL, Hudak Jr SJ. A fracture-mechanics approach to high cycle fretting fatigue based on the worst case fret concept: I. Model development. Int J Fracture 2001;112:299–330.
[3] Chan KS, Davidson DL, Owen TE, Lee YD, Hudak Jr SJ. A fracture-mechanics approach to high cycle fretting fatigue based on the worst case fret concept: II. Experimental evaluation. Int J Fracture 2001;112:331–53.
[4] Endo K, Goto H. Initiation and propagation of fretting-fatigue cracks. Wear 1976;38:311–24.
[5] Fellows LJ, Nowell D, Hills DA. On the initiation of fretting-fatigue cracks. Wear 1997;205:120–9.
[6] Giannakopoulos AE, Lindley TC, Suresh S. Aspects of equivalence between contact mechanics and fracture mechanics: theoretical connections and life-prediction methodology for fretting-fatigue. Acta Mater 1998;46:2955–68.
[7] Giannakopoulos AE, Venkatesh TA, Lindley TC, Suresh S. The role of adhesion in contact fatigue. Acta Mater 1999;47:4653–64.
[8] Juuma T. Torsional fretting-fatigue strength of a shrink-fitted shaft. Wear 1999;231:310–8.
[9] Kondo Y, Bodai M. The fretting-fatigue limit based on local stress at the contact edge. Fatigue Fract Engng M 2001;24:791–801.
[10] Lamacq V, Dubourg MC. Modeling of initial fatigue crack growth and crack branching under fretting conditions. Fatigue Fract Engng M 1999;22:535–42.
[11] Lykins CD, Mall S, Jain VK. A shear stress-based parameter for fretting-fatigue crack initiation. Fatigue Fract Engng M 2001;24:461–73.
[12] Lykins CD, Mall S, Jain VK. Combined experimental-numerical investigation of fretting crack initiation. Int J Fatigue 2001;23:703–11.
[13] Mugadu A, Hills DA. A generalised stress intensity approach to characterising the process zone in complete fretting contacts. Int J Solids Struct 2002;39:1327–35.
[14] Mutoh Y, Xu JQ. Fracture-mechanics approach to fretting fatigue and problems to be solved. Tribol Int 2003;36:99–107.
[15] Nix KJ, Lindley TC. The application of fracture mechanics to fretting fatigue. Fatigue Fract Engng M 1985;8:143–60.
[16] Nowell D, Hills DA. Mechanics of fretting-fatigue tests. Int J Mech Sci 1987;29:355–65.
[17] Rape JA, Neu RW. Influence of contact configuration in fretting-fatigue testing. Wear 1999;225–229:1205–12.
[18] Ruiz C, Boddington PHB, Chen KC. An investigation of fatigue and fretting in a dovetail joint. Exp Mech 1984;24:208–17.
[19] Sato K, Fujii H, Kodama S. Crack propagation behavior in fretting fatigue. Wear 1986;107:245–62.
[20] Sinclair GB, Cormier NG. Contact stresses in dovetail attachments, physical modeling. J Engng Gas Turb Power 2002;124:325–31.
[21] Swalla DR, Neu RW. Influence of coefficient of friction on fretting-fatigue crack nucleation prediction. Tribol Int 2001;34:493–503.
[22] Szolwinski Matthew P, Farris Thomas N. Mechanics of fretting-fatigue crack formulation. Wear 1996;198:93–107.
[23] Waterhouse RB, Taylor DE. The initiation of fatigue cracks in a 0.7% carbon steel by fretting. Wear 1971;17:139–47.
[24] Yang B, Ravi-Chandar K. A single-domain dual-boundary-element formulation incorporating a cohesive zone model for elastostatic cracks. Int J Fracture 1998;93:115–44.
[25] Yang B, Mall S. On crack initiation mechanisms in fretting fatigue. ASME J Appl Mech 2001;68:76–80.